J|A|C|S
ARTICLES
Published on Web 08/20/2005

Chemical Tuning of the Electronic Properties in a Periodic Surfactant-Templated Nanostructured Semiconductor

Scott D. Korlann,[†] Andrew E. Riley,[†] Bradley L. Kirsch,[†] B. Simon Mun,[‡] and Sarah H. Tolbert*,[†]

Contribution from the Department of Chemistry and Biochemistry, University of California at Los Angeles, Los Angeles, California 90095-1569, and Advanced Light Source, Lawrence Berkeley National Lab, Berkeley, California 94720

Received July 28, 2004; E-mail: tolbert@chem.ucla.edu

Abstract: In this work, we report the synthesis and characterization of a series of hexagonal nanostructured platinum/tin/tellurium inorganic/surfactant composites. The composites are formed through solution-phase self-assembly of $SnTe_4^{4-}$ Zintl clusters, which are cross-linked with platinum salts in the presence of a cetyltriethylammonium cationic structure directing agent. The cross-linking utilizes various combinations of Pt(II) and Pt(IV) salts. Low-angle X-ray diffraction indicates that all composites form hexagonal honeycomb (*p6mm*) structures. A combination of elemental analysis and XANES is used to describe the composition and oxidation states within the composites. We find that the extent of tin telluride self-oligomerization and the platinum:tin telluride ratio both vary, indicating that the composite compensates for different platinum oxidation states by tuning the inorganic composition. Near-IR/visible reflectance spectroscopy and UPS can be used to measure both band gaps and absolute band energies. The results show that while moving from all Pt(II) to all Pt(IV) increases the band gap from 0.6 to 0.8 eV, it increases the absolute valence and conduction band energies by almost a full electronvolt. AC impedance spectroscopy further reveals that the conductivities of the materials can be tuned from 0.009 to 0.003 $\Omega^{-1}\cdot cm^{-1}$. Additionally, a capacitance arising from the periodic nanoscale organic domains was observed. The conductivity and band gap were used to estimate carrier mobilities in these composites. Chemical tuning of the electronic properties within related nanostructured composites is a useful tool for designing applications that exploit the properties of nanostructured semiconductors.

Introduction

In the synthesis of periodic inorganic/surfactant composite materials, soluble inorganic precursors coassemble with organic surfactants to form materials with rigid inorganic frameworks and structures reminiscent of liquid crystalline phases. Silica-based materials were among the first synthesized by this method and were also the first where the assembly process was examined.[1−5] Over time, however, the methodology was extended to a wide range of transition metal and main group oxides, such as Al_2O_3, Mn_xO_y, Nb_2O_5, SnO_2, TiO_2, TiO_2/VO_2, ZrO_2, and NiO_2.[6−19] Generally, all of these oxide-based inorganic/organic structures form insulating or wide band gap materials, which are undesirable for applications that require electrical conductivity. Non-oxide materials provide a useful alternative to the insulating oxide systems as they can be produced with band gaps ranging from many electronvolts to less than 1 eV.[20−23] This gives non-oxide materials the potential for much higher intrinsic conductivity than that of main group or transition metal oxide systems.

[†] University of California at Los Angeles.
[‡] Lawrence Berkeley National Lab.

(1) Kresge, C. T.; Leonowicz, M. E.; Roth, W. J.; Vartulli, J. C.; Beck, J. S. *Nature* **1992**, *359*, 710.
(2) Huo, Q.; Margolese, D. I.; Clesa, U.; Feng, P.; Gier, T. E.; Sieger, P.; Leon, R.; Petroff, P. M.; Schuth, F.; Stucky, G. D. *Nature* **1994**, *368*, 317.
(3) Firouzi, A.; Kumar, D.; Bull, L. M.; Besier, T.; Sieger, P.; Hue, Q.; Walker, S. A.; Zasadzinski, J. A.; Glinka, C.; Nicol, J.; Margolese, D.; Stucky, G. D.; Chmelka, B. F. *Science* **1995**, *267*, 1138.
(4) Gross, A. F.; Ruiz, E. J.; Tolbert, S. H. *J. Phys. Chem. B* **2000**, *104*, 5448.
(5) Monnier, A.; Schuth, F.; Huo, Q.; Kumar, D.; Margolese, D.; Maxwell, R. S.; Stucky, G. D.; Krishnamurty, M.; Petroff, P.; Firouzi, A.; Janicke, M.; Chmelka, B. F. *Science* **1993**, *261*, 1299.
(6) Antonelli, D. M.; Ying, J. Y. *Angew. Chem., Int. Ed. Engl.* **1996**, *35*, 426.
(7) Bagshaw, S. A.; Pinnavaia, T. J. *Angew. Chem., Int. Ed. Engl.* **1996**, *35*, 1102.
(8) Tian, Z. R.; Tong, W.; Wang, J. Y.; Duan, N. G.; Krishnan, V. V.; Suib, S. L. *Science* **1997**, *276*, 926.
(9) Ciesla, U.; Schacht, S.; Stucky, G. D.; Unger, K. K.; Schuth, F. *Angew. Chem., Int. Ed. Engl.* **1996**, *35*, 541.
(10) Yang, P. D.; Zhao, D. Y.; Margolese, D. I.; Chmelka, B. F.; Stucky, G. D. *Nature* **1998**, *396*, 152.
(11) Wong, M. S.; Ying, J. Y. *Chem. Mater.* **1998**, *10*, 2067.
(12) Wong, M. S.; Antonelli, D. M.; Ying, J. Y. *Nanostruct. Mater.* **1997**, *9*, 165.
(13) Sun, T.; Ying, J. Y. *Angew. Chem., Int. Ed.* **1998**, *37*, 664.
(14) Linden, M.; Schunk, S. A.; Schuth, F. *Angew. Chem., Int. Ed.* **1998**, *37*, 821.
(15) Pidol, L.; Grosso, D.; Soler-Illia, G.; Crepaldi, E. L.; Sanchez, C.; Albouy, P. A.; Amenitsch, H.; Euzen, P. *J. Mater. Chem.* **2002**, *12*, 557.
(16) Soler-Illia, G.; Louis, A.; Sanchez, C. *Chem. Mater.* **2002**, *14*, 750.
(17) Banjeree, S.; Santhanam, A.; Dhatharthreyan, A.; Rao, P. M. *Langmuir* **2003**, *19*, 5522.
(18) Dong, A.; Ren, N.; Tang, Y.; Wang, Y.; Zhang, Y.; Hua, W.; Gao, Z. *J. Am. Chem. Soc.* **2003**, *125*, 4976.
(19) Yoshitake, H.; Tatsumi, T. *Chem. Mater.* **2003**, *15*, 1695.
(20) Riley, A. E.; Tolbert, S. H. *J. Am. Chem. Soc.* **2003**, *125*, 4551.
(21) Rangan, K. K.; Trikalitis, P. N.; Canlas, C.; Bakas, T.; Weliky, D. P.; Kanatzidis, M. G. *Nano Lett.* **2002**, *2*, 513.
(22) Trikalitis, P. N.; Rangan, K. K.; Kanatzidis, M. G. *J. Am. Chem. Soc.* **2002**, *124*, 2604.
(23) Trikalitis, P. N.; Rangan, K. K.; Bakas, T.; Kanatzidis, M. G. *Nature* **2001**, *410*, 671.

10.1021/ja045446k CCC: $30.25

Scheme 1. Self-Assembly Process for the Formation of Mesostructured Platinum Tin Telluride Composites[a]

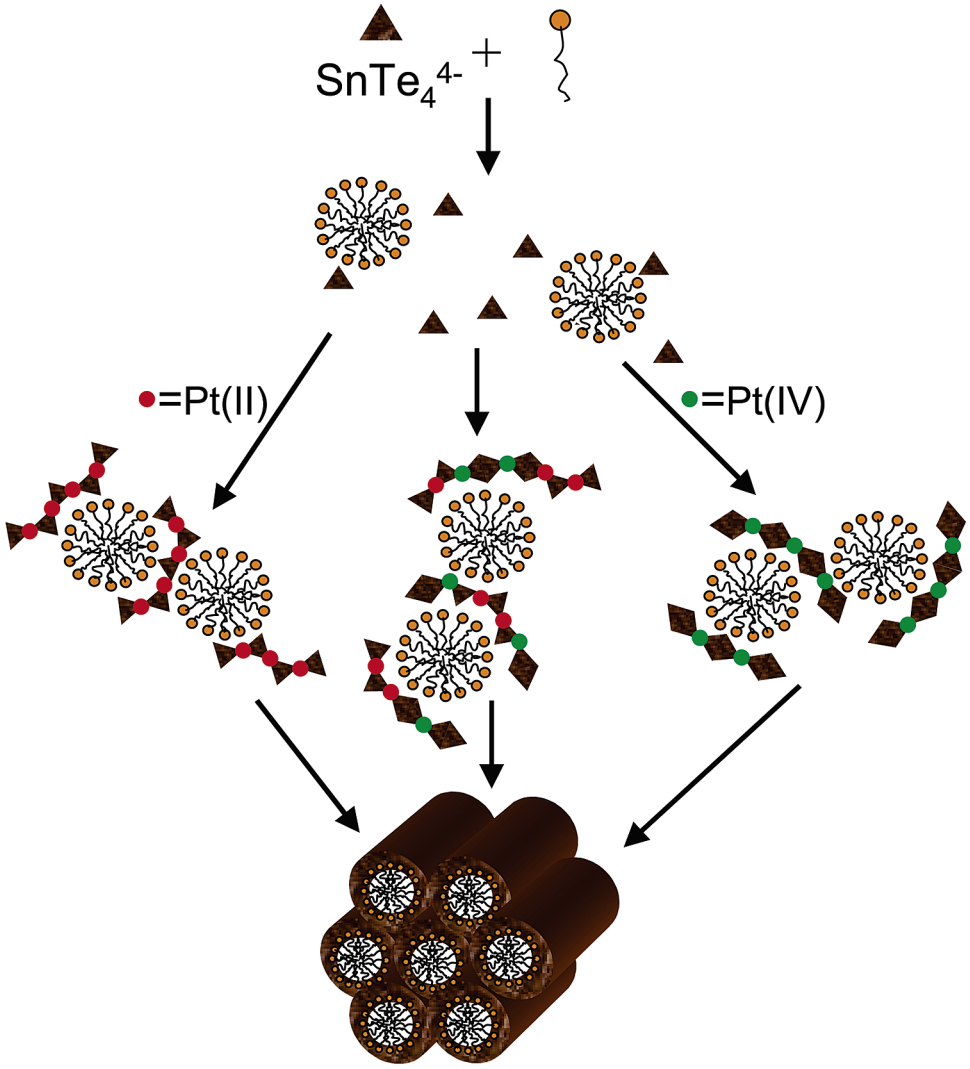

[a] In the first step, the tin telluride Zintl anions and surfactants are dissolved in formamide. In solution, the surfactants form micelles, while the tin telluride monomers are randomly dispersed within the solvent. These monomers are then oligomerized by addition of a cross-linking platinum salt having an oxidation state of either two (red) or four (green). The larger inorganic oligomers associate with the micelles, and oligomerization continues until a complete hexagonal mesostructured network is formed.

To date, self-assembled chalcogenide-based semiconductor composites with a honeycomb architecture have been synthesized with band gaps ranging from 0.8 to 3.4 eV, depending on the framework's chemical components.[20−28] The materials are formed through self-assembly of organic surfactant and main group clusters, termed Zintl ions.[7,29] The Zintl clusters usually contain a mixture of group IV and group VI elements and are polymerized by introducing reactive cross-linking transition metal ions. The resulting electronic structure of these mesostructured materials can be tuned by varying the chalcogenide, the group IV element, or the transition metal used for cross-linking.[20−28] For example, by varying the chalcogenide component of a sample system (Pt−Ge_4Ch_{10}, Ch = chalcogenide), the band gap changes from 2.3 eV (Pt−Ge_4S_{10}) to 1.8 eV (Pt−Ge_4Se_{10}). Furthermore, varying the group IV element from germanium to tin extends this lower band gap range to 1.5 eV (Pt−Sn_4Se_{10}).[22] Further variation in band gaps is possible by changing the cross-linking transition metal. For example, moving from zinc to iron yields band gaps of 2.5 eV (Zn−$SnSe_4$) and 1.4 eV (Fe−$SnSe_4$).[23] The smallest band gap (0.8 eV) reported to date for any periodic inorganic/surfactant composite is that of Pt−$SnTe_4$, cross-linked using Pt(IV).[20]

While a variety of transition metal salts have been used to cross-link chalcogenide-based clusters, platinum has proven to be the most versatile. Platinum(II) salts have been used to form composites with a hexagonal nanoscale morphology by cross-linking $K_4Ge_4S_{10}$, $K_4Ge_4Se_{10}$, K_4SnSe_4, $K_4Sn_2Se_6$, and $K_4Sn_4Se_{10}$ in the presence of surfactant.[21−28] Additionally, platinum(IV) has been used to cross-link K_4SnTe_4.[20] Platinum is the only transition metal that has been reported to form hexagonal composites starting from different oxidation states. The work

(24) Rangan, K. K.; Trikalitis, P. N.; Kanatzidis, M. G. *J. Am. Chem. Soc.* **2000**, *122*, 10230.
(25) Wachhold, M.; Rangan, K. K.; Lei, M.; Thorpe, M. F.; Billinge, S. J. L.; Petkov, V.; Heising, J.; Kanatzidis, M. G. *J. Solid State Chem.* **2000**, *152*, 21.
(26) MacLachlan, M. J.; Coombs, N.; Ozin, G. A. *Nature* **1999**, *397*, 681.
(27) Rangan, K. K.; Billinge, S. J. L.; Petkov, V.; Heising, J.; Kanatzidis, M. G. *Chem. Mater.* **1999**, *11*, 2629.
(28) Trikalitis, P. N.; Rangan, K. K.; Bakas, T.; Kanatzidis, M. G. *J. Am. Chem. Soc.* **2002**, *124*, 12255.
(29) Kauzlarich, S. M. *Chemistry, Structure, And Bonding Of Zintl Phases And Ions*; VCH: New York, 1996.

on smaller clusters with platinum(II) suggests that it should be possible to synthesize the Pt−$SnTe_4$ system with platinum(II) as well as the previously reported platinum(IV).[29]

In this paper, Pt−$SnTe_4$ inorganic/surfactant self-assembled structures have thus been formed by cross-linking K_4SnTe_4 clusters with various mixtures of platinum salts, as shown in Scheme 1. Composites were synthesized with Pt(II), Pt(IV), and various mixtures of these two salts. The goal of mixing the Pt(II) and Pt(IV) precursor salts was to obtain a series of hexagonal self-assembled semiconductors using the same elements, but with different overall compositions. The electronic properties of this series of materials were then probed in an effort to correlate the synthetic chemistry with their final electronic properties. The Pt−$SnTe_4$ inorganic/organic composite system, in particular, was chosen because it is a narrow band gap semiconductor which should show moderate conductivity that should be very sensitive to changes in the electronic structure. Moreover, synthetically, it is the only system currently reported to form hexagonal composites with platinum(IV). We find that the synthetic method of tuning the oxidation state of the starting materials allows for control of the band gap, the conductivity, and the absolute energy levels of the final nanoperiodic composite.

Experimental Section

Cetyltriethylammonium bromide (CTEAB) was used as a structure-directing agent in the solution-phase synthesis of these inorganic/organic composite materials. This surfactant was synthesized by reaction of triethylamine (Acros) with 1-bromohexadecane (Acros) in ethanol, as previously reported.[20,30]

All composite syntheses and manipulations were carried out under inert atmosphere to prevent oxidation. K_4SnTe_4 was synthesized according to established methods.[20,31] In the first step, equimolar quantities of potassium (Aldrich) and tin (Acros) were alloyed followed by an exothermic alloying step of equimolar quantities of KSn with tellurium (Acros). The products were solid K_4SnTe_4 and tin. The product, K_4SnTe_4, was extracted using degassed water. The aqueous solution was filtered under inert conditions, evaporated under vacuum, and finally washed with acetone to yield a dark-red powder.

The mesostructured platinum tin telluride composites were synthesized using a solution-phase methodology. A metal cluster/surfactant solution was made by adding 0.25 mmol of K_4SnTe_4 and 0.48 mmol of CTEAB surfactant to 17.7 mmol of formamide (Alfa Aesar). Next, a solution of cross-linking agent was prepared by adding 0.2 mmol of platinum salts to 17.7 mmol of formamide (Alfa Aesar). The platinum salts, $PtCl_4$ (Aldrich) and K_2PtCl_4 (Alfa Aesar), were dissolved in formamide to form a mixture of platinum salts with oxidation states Pt(IV):Pt(II) in varying ratios. The molar amount of platinum, however, was constant across all synthesis solutions. Both solutions were then heated to 66 °C, and the platinum solution was added to the tin telluride solution while stirring. The temperature of the mixture was maintained for 10 min, during which time an appreciable amount of precipitate formed. The precipitate was transferred to a fritted filter and then rinsed dropwise with at least 20 mL of formamide to remove any residual surfactant. Finally, the mesostructured composites were dried for 14 h under vacuum and better than 30 mTorr to evaporate the excess formamide. Composites with molar ratios of 0:4, 1:3, 2:2, and 4:0 [Pt(IV):Pt(II)] were produced.

Carbon, hydrogen, and nitrogen contents were determined by Desert Analytics (P.O. Box 41838, Tucson, AZ 85717). Platinum, tin, and tellurium contents were determined by either Desert Analytics or in house using a Jarrell Ash Iris 1000 inductively coupled plasma spectrometer (ICP). Prior to sample digestion, the composite material was weighed in a flask under inert atmosphere. In the first step of the digestion, an acidic solution (2 HCl:1 HNO_3) was transferred into the flask. The acidic solution was then refluxed for at least 2 h. After cooling, the solution (containing some solid) was adjusted to pH 12 by addition of 5 M NaOH. The solution was then refluxed again for at least 2 h to dissolve the residual solids. This solution was then diluted to known volume and run through a 0.22 μm PTFE filter.

X-ray diffraction was performed using a Rigaku UltraX 18 rotating anode X-ray source providing Mo Kα radiation equipped with a Roper Scientific 1242 × 1156 pixel X-ray CCD detector. Diffraction data were collected in a transmission geometry. All samples were sealed under argon between two Mylar windows to prevent oxidation.

X-ray absorption near edge spectroscopy (XANES) was performed on beam line 10-2 at the Stanford Synchrotron Radiation Laboratory (SSRL). Samples were sealed within Mylar sheets under inert atmosphere and held in a liquid helium-cooled cryostat at 100 K. The data were collected in absorption geometry. A Si(220) phi 90° monochromator crystal was used with 2 mm vertical and 10 mm horizontal slits. The accumulation time was 1 h per scan with a 0.35 eV step size over a 1 keV range, allowing 1.25 s/step. For each element, a standard was used to compensate for slight energy shifts of the beam. The standards used were Pt foil (L_3, 11 564 eV), Te powder (Acros) (K, 31 814 eV), and Sn foil (K, 29 200 eV). For data analysis, the position of the edge was assigned to the inflection point in the absorption edge, which was determined by finding the peak of the 2nd derivative taken in the region of the absorption edge.

Near-IR/UV−visible diffuse reflectance measurements were taken on a Shimadzu UV−3100 spectrometer. Due to the high optical density of the samples, spectra were taken in reflectance geometry using an ISR-3100 integrating sphere attachment. The spectra were collected over the range of 400−2400 nm. Thin samples were sealed between two borosilicate microscope slides and placed in front of a $BaSO_4$ background to prevent oxidation.

Impedance spectroscopy was performed using a 4284A HP impedance analyzer. Samples were compacted and measured in a gastight inert polycarbonate cell with a known volume that was comprised of a 0.027 cm^2 cross-sectional area and a 0.155 cm length. The samples were contacted by machined stainless steel pins. The impedance analyzer calibration was checked using a 1 ohm ± 1% metal film resistor prior to taking measurements. All samples were measured with a 150 mV potential applied to the sample. X-ray diffraction was taken on all samples after the impedance measurements were taken to ensure the nanoscale order was not harmed by the measurement. The experimental data were modeled with Zsimpwin (version 2.0, EChem Software).

Ultraviolet photoelectron spectroscopy (UPS) was performed on beam line 9.3.2 at the Advanced Light Source, at Lawrence Berkeley National Laboratory. To prevent charging, the powder samples were mixed in a 1:1 ratio with a carbon black powder, which is a good conductor. Next, the sample powder was pressed into indium foil, and a silver paste contact was made at the edge of the sample to ensure good electrical contact to the sample holder. All samples were handled and loaded into the UPS chamber under inert atmosphere. The experiment was run under ultrahigh vacuum conditions ($\sim 10^{-9}$ Torr). All samples were exposed to incident photons with an energy of 105.1 eV, and the kinetic energies of electrons ejected from the valence band were measured. In all experiments, the valence band energy was determined relative to the work function of gold foil (5.1 eV);[34] the

(30) Menger, F. M.; Littau, C. A. *J. Am. Chem. Soc.* **1993**, *115*, 10083.
(31) Hauffman, J. C.; Haushalter, J. P.; Umarji, A. M.; Shenoy, G. K.; Haushalter, R. C. *Inorg. Chem.* **1984**, *23*, 2312.
(32) *Impedance Spectroscopy: Emphasizing Solid Materials and Systems*, 3rd ed.; Macdonald, J. R., Ed.; Wiley: New York, 1987.
(33) Campbell, J.; Devereux, L.; Gerken, M.; Mercier, H.; Pirani, A.; Schrobilgen, G. *Inorg. Chem.* **1996**, *35*, 2945.
(34) *CRC Handbook of Chemistry and Physics*, 81st ed.; Lide, D. R., Ed.; CRC Press: Boca Raton, FL, 2000.

gold standard was cleaned by argon-ion sputtering at room temperature under UHV conditions.

Results

1. Synthesis, Low-Angle X-ray Diffraction, and X-ray Absorption Analysis. During the synthesis of platinum tin telluride mesostructures, the inorganic/organic self-assembly is driven by electrostatic attraction. CTEAB micelles and Zintl clusters (K_4SnTe_4) form a stable solution in formamide. The role of the cross-linking transition metal ion is to oligomerize the Zintl clusters into polymeric species. This lowers the entropic penalty associated with aggregation between the surfactant micelles and the inorganic species, which in turn leads to assembly and precipitation of a nanostructured composite.[5]

As discussed previously, Zintl cluster-based inorganic/organic composites with nanoscale periodicity can be synthesized using either platinum(II) or platinum(IV) salts as cross-linking agents.[20−28] Alternatively, mixtures of these salts can also be used to synthesize nanostructured composites. By controlling the ratio of the two platinum salts, the net oxidation state of the final self-assembled structure can be systematically varied. To ensure that the final composite contained a mixture of platinum salts that was similar to the starting solution, the reaction yield was visually observed to determine the temperature where both cross-linking platinum salts, $PtCl_4$ and K_2PtCl_4, reacted at similar rates. Below 60 °C, a Zintl/surfactant solution with only the Pt(IV) salt added formed a platinum tin telluride inorganic/surfactant composite precipitate with hexagonal structure. However, no precipitate was observed for a solution containing only the Pt(II) salt. Between 60 and 65 °C, a precipitate formed using the Pt(II) salt, but the material lacked hexagonal structure, as indicated by low-angle XRD. Both Pt(II) and Pt(IV) solutions, however, react within 1 min at 66 °C to form a precipitate with hexagonal order. After 10 min, a large amount of precipitate formed for both Pt(IV) and Pt(II) salt solutions. After filtration and vacuum-drying, the synthesis using the Pt(II) cross-linking salt yielded 96 mg of composite, while the synthesis using the Pt(IV) cross-linking salt yielded 109 mg of composite. The weight of these products is similar, verifying that their composite assembly rates over the 10 min time scale are similar. These observations suggest that a solution containing a homogeneous mixture of the two cross-linking platinum salts should incorporate both platinum ions into the inorganic platinum tin telluride mesostructure.

Low-angle X-ray diffraction data (Figure 1) show *p*6*mm* two-dimensional hexagonal order for all the composites, regardless of the Pt(IV):Pt(II) molar ratio. The diffraction patterns show peaks in a position ratio of $1:\sqrt{3}:2$, which corresponds to the (10), (11), and (20) diffraction peaks. The hexagonal lattice parameter (a) is similar for all of the composites and falls in the range of 44 ± 0.6 Å. This compares well to the lattice parameter previously reported for the pure Pt(IV) composite (43 Å) using both low-angle XRD and transmission electron microscopy (TEM).[20] No obvious trend in the lattice constant with varying Pt(IV):Pt(II) ratio was observed. The d-spacing and hexagonal nature indicate that this series of materials maintains similar structure on the nanometer length scale regardless of the platinum salt used.

X-ray adsorption near-edge spectroscopy (XANES) can be used to determine the oxidation states of elements within a molecular structure. In a XANES experiment, high-energy X-rays ionize core level electrons of the elemental components of interest. The energy at which an element shows an X-ray absorption step is dependent on the oxidation state of the element. The greater the oxidation state of an element in a molecular framework, the more energy it generally takes to ionize a core level electron of that element. The difference in energy of the absorption edge for a given element in a sample with respect to a standard with known oxidation state (usually the pure element) can be used to determine the shift in the absorption edge, ΔE_o. K_4SnTe_4 Zintl precursor clusters ideally contain four Te^{2-} and one Sn^{4+}. However, covalency reduces the formal charge on Te toward Te^{1-} and Sn toward Sn^0. The platinum cross-linking salts clearly initially contain either Pt^{2+} or Pt^{4+} or a mixture of the two. In solution or in the composite, however, these oxidation states can change due to redox chemistry.[32] Therefore, we use a combination of elemental analysis and XANES data to draw conclusions about the final oxidation states of these elements in the solid-state $Pt-SnTe_4$ hexagonal inorganic/organic composites and, hence, the redox chemistry that occurs during formation of the final product.

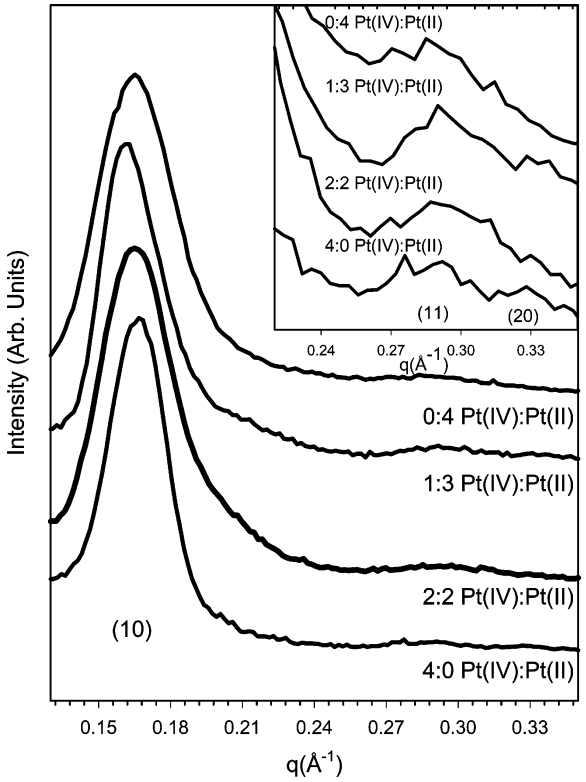

Figure 1. Low-angle X-ray diffraction for mesostructured platinum tin telluride inorganic/surfactant composites synthesized using Pt(IV):Pt(II) molar ratios of 0:4, 1:3, 2:2, and 4:0. The (10) fundamental peak and (11) overtone peak of a hexagonal phase are observed in the X-ray diffraction for all of the platinum tin telluride composites. In the 4:0 platinum tin telluride composite, a (20) is also observed. As the ratio of Pt(II) is increased, the (20) peak becomes less apparent. The structure of these mesostructured composites is a *p*6*mm* two-dimensional hexagonal lattice, with (10), (11), and (20) peak position ratios of $1:\sqrt{3}:2$.

The shifts of the edges observed in the absorption spectrum for the elements Pt, Te, and Sn in our mesostructured composites are seen in Figure 2. For the entire series of mesostructured platinum tin telluride composites (Pt(IV):Pt(II) with molar ratios of 0:4, 1:3, 2:2, and 4:0), the tellurium absorption edge is shifted from the absorption edge of the tellurium standard by a constant

Table 1. Summary of Elemental Analysis[a]

Pt(IV):Pt(II) molar ratio	sample composition normalized to Sn	sample composition normalized to CTEA	Pt:Sn	Te:Sn	CTEA:Sn
0:4	$CTEA_{1.2}Pt_{1.3}Sn_{1.0}Te_{4.5}$	$CTEA_{1.0}Pt_{1.9}Sn_{1.4}Te_{6.6}$	1.3	4.5	1.2
1:3	$CTEA_{0.9}Pt_{1.1}Sn_{1.0}Te_{4.2}$	$CTEA_{1.0}Pt_{1.2}Sn_{1.1}Te_{4.7}$	1.1	4.2	0.9
2:2	$CTEA_{0.9}Pt_{0.8}\ Sn_{1.0}Te_{3.6}$	$CTEA_{1.0}Pt_{0.9}Sn_{1.1}Te_{4.0}$	0.8	3.6	0.9
4:0	$CTEA_{1.0}Pt_{0.5}Sn_{1.0}Te_{3.5}$	$CTEA_{1.0}Pt_{0.5}Sn_{1.0}Te_{3.5}$	0.5	3.5	1.0

[a] Elemental compositions of the various platinum tin telluride composites. Potassium and chlorine were not present in any of the samples analyzed and thus are not included in this table.

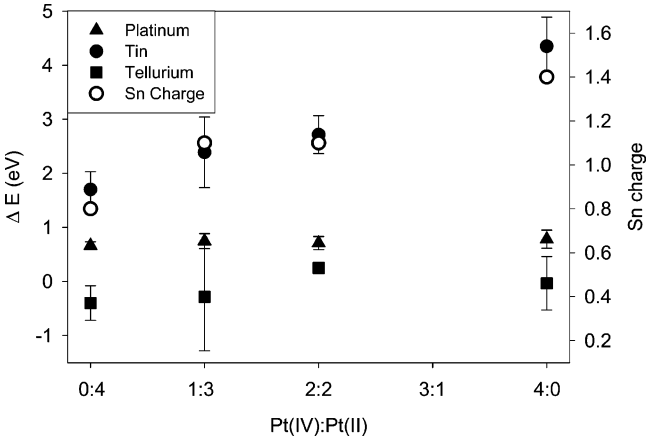

Figure 2. Average shift of the X-ray absorption edge observed for the elements Pt, Te, and Sn in mesostructured platinum tin telluride inorganic/surfactant composites as a function of the Pt(IV):Pt(II) molar ratio used in the synthesis. The data indicate that the final platinum and tellurium oxidation states stay constant for all composites. The tin edge shifts to higher energies as the Pt(IV):Pt(II) ratio is increased, indicating that tin is oxidized as more Pt(IV) is added. The charge of the tin atom, as calculated from elemental ratios, is also plotted and shows good agreement with the XANES data.

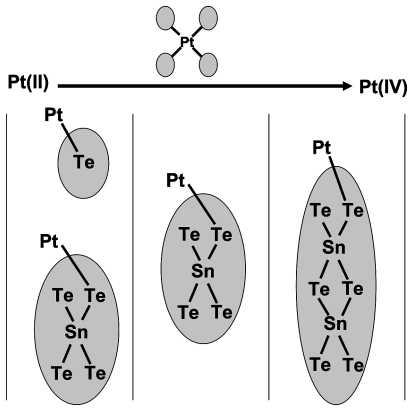

Figure 3. A summary of the types of bonding motifs found in hexagonal surfactant-templated inorganic composites made from $SnTe_4^{4-}$ ions coupled together with different ratios of Pt(II) and Pt(IV). As the fraction of Pt(IV) used to synthesize the mesostructured composite increases, the extent of tin telluride self-oligomerization also increases. This results in elemental compositions higher in tin and lower in tellurium and platinum for materials made exclusively with Pt(IV).

amount, -0.1 ± 0.3 eV. Therefore, the tellurium in these materials maintains a consistent shift, indicating that it is fairly inflexible in terms of its oxidation state On the basis of redox potentials, this oxidation state is probably Te^{1-}. For the entire series of composite materials (Pt(IV):Pt(II) with molar ratios of 0:4, 1:3, 2:2, and 4:0), the platinum absorption edge is also shifted from the absorption edge of platinum foil by a constant amount, 0.72 ± 0.07 eV. The Pt(II) standard, $PtCl_2$, shows an edge shift of 0.8 eV. This indicates platinum is likely reduced to Pt(II) in the final material, regardless of what ratio of Pt(IV):Pt(II) salts are used for cross-linking. By contrast, the tin absorption edges in the composites continually shift to higher energy with respect to the absorption edge of the tin standard as the amount of Pt(IV) in the synthesis solution is increased, indicating a steadily increasing oxidation state with increasing Pt(IV) content.

The elemental compositions of a series of Pt couple $SnTe_4^{4-}$ hexagonal composites made with varying Pt(IV):Pt(II) ratios are shown in Table 1. Potassium and chlorine were not present in any of the samples analyzed and thus are not included in this table. It should also be noted that the organic component of these samples is comprised of both the cetyltriethylammonium cation ($CTEA^+$) and residual solvent. The amount of surfactant in the material is calculated from the weight percentages of C, H, and N.[20] The compositions of the samples are given in Table 1. A great deal about the structure can be inferred from the elemental data, including information about the structure of the Zintl cluster in the final material (tin-to-tellurium ratio), the extent of cross-linking through the transition metal (platinum to tin), and the role of the organic in charge balancing the inorganic framework (CTEA to tin).

The tin-to-tellurium ratio in these materials describes the extent of self-oligomerization the $SnTe_4^{4-}$ anion undergoes during the process of assembly. This self-oligomerization is a separate process from the transition-metal-induced cross-linking. In solution, $SnTe_4^{4-}$ can eliminate soluble tellurides to form either $Sn_2Te_7^{4-}$ or Sn_2Te_6.[4-33] In this series of composites, the 0:4, 1:3, 2:2, and 4:0 [Pt(IV):Pt(II)] materials have Te:Sn ratios of 4.5, 4.2, 3.6, and 3.5, respectively (Table 1). The general trend in these data is that as more Pt(IV) is added to the synthesis mixture, the extent of tin telluride oligomerization becomes larger. It appears that while the platinum is a cross-linking agent, depending on its oxidation state, the Pt or the Cl^- counterions it generates also help drive the tin telluride oligomerization.[31] A possible mechanism for this process relies on the electron-deficient nature of Pt(IV). As a result, the tellurium may form more bridging bonds with tin to accommodate the lack of electrons. The formation of bridging bonds is facilitated by expulsion of some tellurium from the framework. It should also be noted that the 0:4 and 1:3 [Pt(IV):Pt(II)] samples have Te:Sn ratios that are higher than those of the monomeric $SnTe_4^{4-}$ cluster. Tellurium rearrangement may also explain this occurrence— Pt−Te bonds are quite strong, and it is quite possible that platinum may be coordinated by a combination of clusters and other soluble telluride anions.[34] A summary of the most common bonding motifs found in each composite is presented in Figure 3.

The platinum-to-tin ratio for the series shows a decrease with increasing Pt(IV) content used in the synthesis, indicating that charge balancing in the composite is accomplished both by the

cationic surfactant and by the cross-linking agent. The lower charge on platinum(II) requires more platinum to balance the anionic charge, leading to materials with a high extent of oligomerization from metal-induced cross-linking. By contrast, a composite that is synthesized with a platinum(IV) salt needs less transition metal to balance the anionic charge on the Zintl cluster and thus uses more tin telluride self-oligomerization to form an extended network. The elemental trends illustrate the competition between these two oligomerization routes (metal cross-linking and cluster self-oligomerization), which allows us to form a continuous series of stable composites made with the same elements, but having continually varying stoichiometry.

The combination of XANES and elemental analysis also provides insight into oxidation states of the final materials. XANES (Figure 2) indicates that the platinum oxidation state stays nearly constant at a charge of Pt^{2+}, and the tellurium oxidation state also stays constant, presumably at a charge of Te^{1-} (see below). By contrast, the tin charge in these materials varies continuously with Pt(IV) content. The actual charge per tin atom was calculated to be +0.8, +1.1, +1.1, and +1.5 for the 0:4, 1:3, 2:2, and 4:0 [Pt(IV):Pt(II)] composites, respectively, using the elemental ratios, the previously described charges for platinum (2+), tellurium (1−), and surfactant (1+), and the assumption of charge neutrality. These numbers agree well with the XANES data for tin, as the trend in the edge tracks the increase in tin charge almost exactly (Figure 2).

In the end, it appears that all of the oxidation state data on these nanoscale inorganic materials can be understood using standard solution-phase reduction potentials. The oxidation of Te^{2-} to Te^{1-} has a large positive potential of 1.45 V.[35] The reduction of Pt(IV) to Pt(II) is also positive ($PtCl_6^{2-} + 2e^- \rightarrow PtCl_4^{2-} = 0.73$ V).[36] The tin species has two potentially applicable half-reactions ($Sn^{2+} + 2e^- \rightarrow Sn = -0.137$ V, $Sn^{4+} + 2e^- \rightarrow Sn^{2+} = 0.15$ V), both of which show very small potentials. Thus, while both Sn^{2+} oxidation and reduction have negative potentials, they are both low-energy processes. Comparing the potentials for Sn and Te, it is clear that Sn should be preferentially oxidized to balance the Pt reduction in composites synthesized using Pt^{4+}, a trend which is, in fact, observed. The final oxidation states of the material thus show the ability to tune the oxidation state of the most flexible atomic components while maintaining the same mesoscale periodicity in the inorganic framework.

2. Optical Band Gap. Reflectance spectra taken of the semiconducting platinum tin telluride composites can be used to determine the optical band gaps of these materials. The band gaps are determined by fitting the linear portion of the absorption edge of a Tauc plot (Figure 4) and extrapolating the fit to the intercept of the energy axis.[37,38] The energy at this intercept is the optical band gap of the mesostructured platinum tin telluride samples and is tabulated in Table 2. This method is commonly used to find the band gap of amorphous semiconductors.[39] The series of materials in Figure 4 shows that as the percentage of Pt(IV) incorporated in the platinum tin telluride inorganic/organic composite is increased, the band gap smoothly shifts to higher energy. It should also be noted that the 0:4 Pt(IV):Pt(II) Pt−$SnTe_4$ composite has a band gap of 0.57 V, which is the smallest band gap reported for a periodic solution-phase-assembled mesostructured inorganic/surfactant composite to date.[20−28]

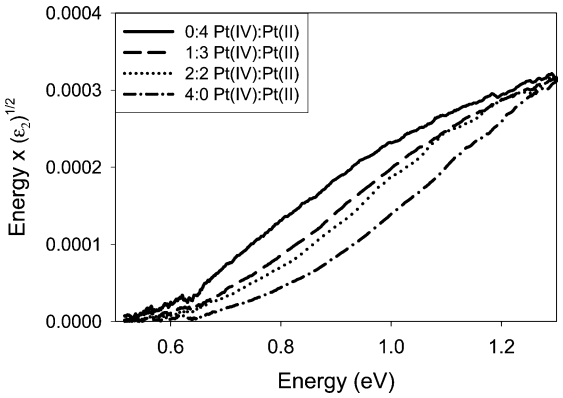

Figure 4. Tauc plots of near-IR/UV−visible diffuse reflectance data for semiconducting platinum tin telluride inorganic/surfactant composites synthesized with various molar ratios of Pt(IV):Pt(II). ϵ_2 is the imaginary part of the dielectric constant and is related to the adsorption coefficient (α) ($\alpha = \epsilon_2 4\pi/2n\lambda$).[38] The band gap is assigned to the intercept of the energy axis with a linear fit to the Tauc curve.[37] As the Pt(IV) content is increased in the synthesis mixture, the band gap becomes larger.

Table 2. Summary of Optical Band Gap Data[a]

Pt(IV):Pt(II) molar ratio	band gap (eV)
0:4	0.57
1:3	0.65
2:2	0.69
4:0	0.75

[a] Optical band gaps obtained from a Tauc plot of near-IR/UV−visible diffuse reflectance data for the platinum tin telluride composites made with varying Pt(II):Pt(IV) ratios. The band gaps were determined by fitting the linear portion of the absorption edge in a Tauc plot (Figure 4) and extrapolating the linear fit to the intercept of the energy axis. As the Pt(IV) content of the synthesis mixture is increased, the band gap increases.

3. AC Impedance Spectroscopy and Conductivity. Impedance spectroscopy is used to determine the conductivity of the semiconducting platinum tin telluride composites in the series. Because these materials are produced as powders, direct current techniques cannot be applied to measure their resistance. The grain boundary contribution to the resistance dominates the measured value, masking the inherent resistance of the semiconducting framework. Impedance spectroscopy can be used to separate the grain boundary contribution from the intrinsic sample resistance through the application of variable frequency current. This technique takes advantage of differing capacitive time constants to isolate various circuit elements. At higher frequencies, charging at the grain boundaries is limited, and the sample resistance is the dominant contributor to the resistivity.

The impedance spectra for the various Pt couple $SnTe_4^{4-}$-based composites, appearing as domes or arcs, are shown in Figure 5a and b, respectively. The grain boundary resistance is the dominant contribution in the high-resistance, low-frequency portion of the impedance spectrum in both Figure 5a and b. The arcs are truncated domes and stem from samples where the Pt−$SnTe_4$ mesostructured composite has a larger grain

(35) Charlot, G.; Marie, C. International Union of Pure and Applied Chemistry. *Selected Constants: Oxydo-Reduction Potentials*; Pergamon: New York, 1958.
(36) While both of these half-reactions are not the exact species in our synthesis, they indicate the magnitude of difference between the two species.
(37) Tauc, J.; Grigorovici, R.; Vancu, A. *Phys. Status Solidi* **1966**, *15*, 627.
(38) Rantzer, A.; Arwin, H.; Birch, J.; Hjorvarsson, B.; Bakker, J. W. P.; Jarrendahl, K. *Thin Solid Films* **2001**, *394*, 256.
(39) Kozlowski, M. R.; Tyler, P. S.; Smyrl, W. H.; Atanasoki, R. T. *Surface Sci.* **1988**, *194*, 505.

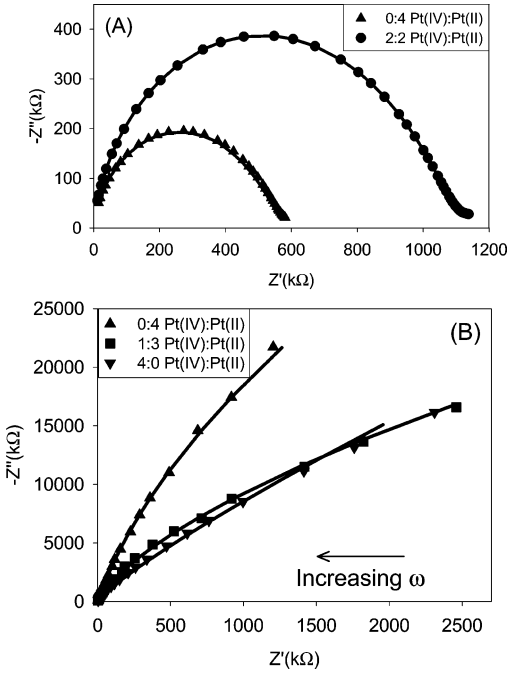

Figure 5. Impedance spectra of mesostructured platinum tin telluride inorganic/surfactant composites synthesized with various Pt(IV):Pt(II) molar ratios. The experimental data are plotted as points, while the simulated impedance spectra for these compounds are plotted as curves. When the alternating current (ac) frequency is increased, the real impedance (Z') is decreased and the imaginary impedance (Z'') results in domes (part a) or arcs (part b) that approach the intrinsic resistance of the sample. The intrinsic sample resistance is the major component of the resistance signal at high ac frequencies.

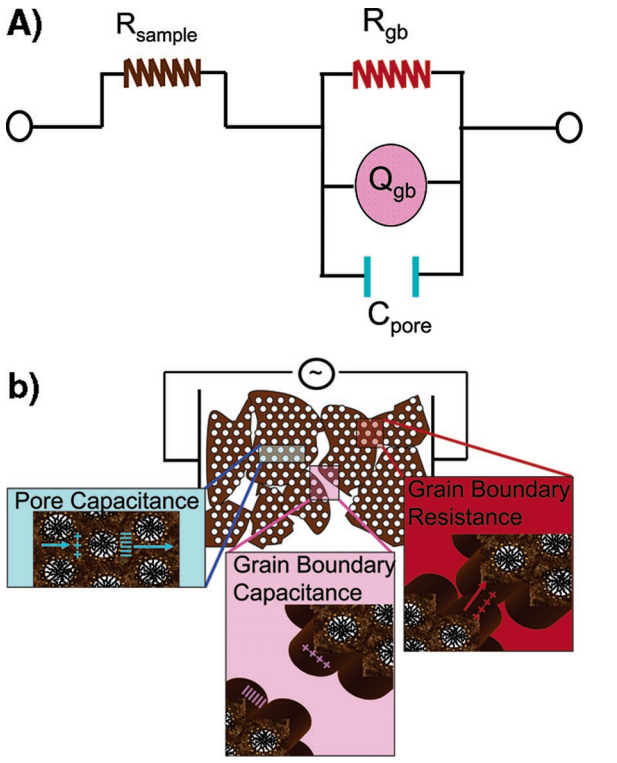

Figure 6. Part (a) shows the equivalent circuit used to model current flow through the mesostructured platinum tin telluride inorganic/surfactant composites. R_{sample} is the intrinsic resistance of the sample. R_{gb} is the resistance of grain boundary contacts. Q_{gb} is a constant phase element representing the capacitance of the grain boundaries. The constant phase element is necessary to represent the variety of grain contacts in the material. C_{pore} is the capacitance of the organic containing pores. Part (b) shows a cartoon depiction of the current flow through the composite, illustrating each of the circuit elements shown in part (a). Sample resistance occurs when current is conducted through the brown sample while staying within a single grain. Capacitance at grain boundaries or at the inorganic/organic interface and resistive hopping between grains result in other impedance effects.

boundary resistance compared to that of composites that exhibit domes. The variation is not systematic and likely stems from differences in packing density, grain size, or surface oxidation. If the measurements were extended to lower frequency, it is expected that the arcs would show full domes. In agreement with this idea, highly consistent values of the intrinsic sample resistance are obtained from both dome and arc data.

Intrinsic sample resistances can be obtained from the high-frequency, low-resistance region of the plots. However, due to instrumental limitations, our impedance spectra never intersect the real impedance axis (Z'); therefore, the intrinsic sample resistance cannot be directly obtained from this intercept. Instead, it must be fit using the circuit model, as depicted in Figure 6. The equivalent circuit is an arrangement of the different circuit elements in a manner that represents electron flow through these materials. When a potential is applied across our sample, an electron first has to travel through the sample, resulting in the initial sample resistance term. After this process, the electron can become trapped at a grain boundary capacitor or travel through a resistive grain boundary. Because of the unique nanoscale structure of these materials, the electron can also associate with the boundary of an organic domain, producing what we call a pore capacitance. In Figure 6, the grain boundaries are modeled as an imperfect capacitor known as a constant phase element. The constant phase element is an empirically determined circuit element that produces an impedance spectrum which appears to be a depressed semicircular dome (Figure 5a).[40,41] The constant phase element can be viewed as a distribution of capacitors, which corresponds to a distribution of grain boundary shapes and separations. Because any given conduction electron will sample either the pore capacitance (C_{pore}), the grain boundary capacitance (C_{gb}), or the grain boundary resistance (R_{gb}), these terms are all in parallel in the equivalent circuit, while the sample resistance (R_{sample}) is in series with all of them. We note that while the grain boundary capacitance is modeled as a distribution of capacitors, this distribution cannot cover both the grain boundary and the pore capacitance. In general, the distribution width is not excessively large ($\alpha_{ave} = 0.27$), and the average value of the grain boundary resistance is 2 orders of magnitude large than the pore capacitance ($C_{gb,ave} = 1.7 \times 10^{-10}$ C; $C_{pore,ave} = 1.67 \times 10^{-12}$ C). Thus, two distinct circuit elements are needed to describe the overall trends in the data.

The simulated impedance spectra of the equivalent circuit show good agreement with the experimental data in Figure 5a and b. The model derived from the equivalent circuit (Figure 6) is robust and able to fit all observed spectra, including both arcs and domes. Additionally, several alternative models have been constructed that did not yield physically reasonable numbers (e.g., negative resistances) or were not able to fit the data well.

As shown in Figure 7, the conductivity of our semiconducting platinum tin telluride composites decreases as the molar ratio

(40) Lang, G.; Heusler, K. E. *J. Electroanal. Chem.* **1998**, *457*, 257.
(41) Cole, S. C.; Cole, R. H. *J. Chem. Pys.* **1941**, *9*, 341.

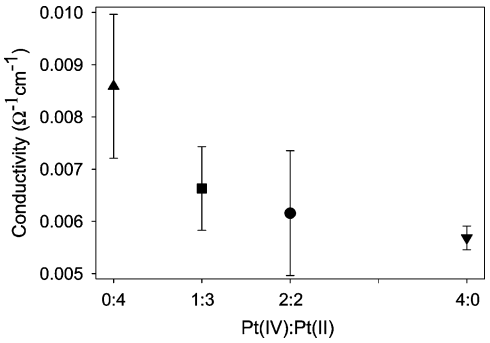

Figure 7. The intrinsic conductivity of the mesostructured platinum tin telluride inorganic/surfactant composites as a function of the Pt oxidation state used in the synthesis. The conductivity plotted is an average of the intrinsic sample resistances obtained by fitting all of the impedance spectra, both arcs and domes. As the amount of Pt(IV) in the synthesis solution is increased, the conductivity of the nanoscale composite material decreases, which is attributed in part to less thermal population of the conduction band with increasing band gap.

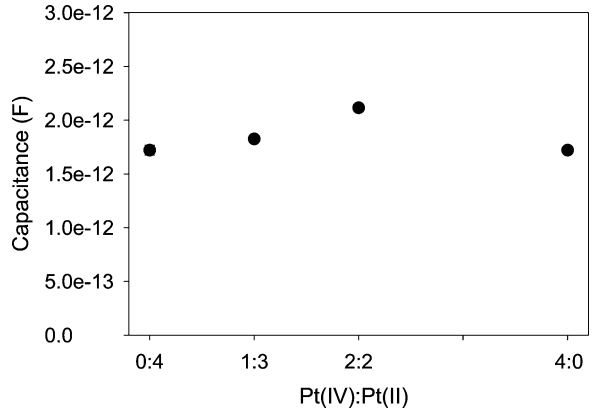

Figure 8. Pore capacitance arising from the nanoscale architecture in the platinum tin telluride inorganic/organic composites. The organic structure directing agent serves as a dielectric embedded in the semiconducting platinum tin telluride framework. The pore capacitance stays nearly invariant over all of the composites with an average value of 1.8×10^{-12} F for all of the data presented here, both arcs and domes. The small fluctuations in pore capacitance may be attributed to varying amounts of formamide embedded inside in the nanoscale semiconductor composite framework, a hypothesis which is consistent with elemental analysis data.

of Pt(IV) is increased. Combining Figure 4 and Figure 7 shows that as the band gap increases, the conductivity in these composites decreases. This inverse relation between the band gap and the conductivity implies that conductivity in these materials is related to the thermally excited carrier population. The conductivities of the platinum tin telluride mesostructured inorganic/organic composites (0.0086−0.0057 $\Omega^{-1}\cdot$cm^{-1}) and their respective band gaps (0.57−0.75 eV) are similar to that of the amorphous semiconductor germanium, which has a conductivity of 0.013 $\Omega^{-1}\cdot$cm^{-1} and a band gap of 0.88 eV.[37,42] Additionally, the pore capacitance is found to have a fairly constant value of $(1.8 \pm 0.1) \times 10^{-12}$ F (Figure 8). This value agrees reasonably well with the calculated pore capacitance of 1×10^{-12} F, which is described in further detail below.

4. Absolute Energy Levels and Electronic Structure. Ultraviolet photoelectron spectroscopy can be used to determine the absolute energy of the valence band edges of the semiconducting platinum tin telluride composites. The valence band edge is found by fitting the linear portion of the photoelectron

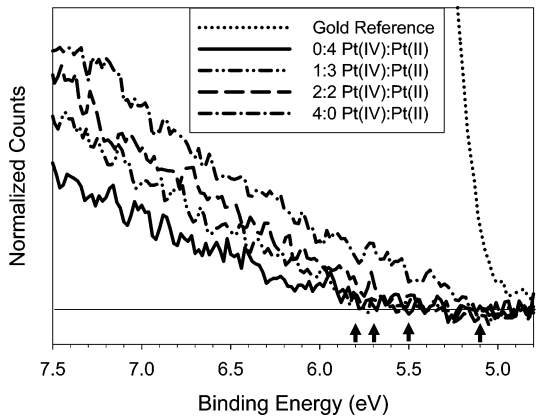

Figure 9. Ultraviolet photoelectron spectra of the mesostructured composites synthesized using various Pt combinations of Pt(II) and Pt(IV) salts. The binding energy is shown with reference to the vacuum level ($E = 0$). The valence band edge was assigned to be the intercept of a linear extrapolation of the band edge with the baseline (see arrows). The absolute energy of the samples valence band edge was determined by comparing the band edge to a standard gold valence band edge. As the amount of Pt(IV) incorporated into the mesostructured composite is increased, the valence band edges shift to higher energies.

spectrum (Figure 9) near the band edge and extrapolating the fit to the intercept with the baseline. To assign the absolute energy of the composite valence band edge, the energy of the valence band was referenced to the gold Fermi level, which is known to have a binding energy of 5.1 eV.[34] The series of materials in Figure 9 exhibits a systematic valence band shift to higher binding energies and lower absolute energies as the amount of Pt(IV) incorporated in the mesostructured composite is increased.

Discussion

One advantage of Zintl clusters as building blocks for self-assembled surfactant-templated mesostructured systems is that they have compositional flexibility. The Pt−$SnTe_4$ Zintl system described in this paper exhibits tunable electronic properties when the ratio of oxidation states of the platinum cross-linking salts in the synthesis mixture is varied. An interesting trend is that the elemental composition of the composites seems to adjust in different ways to accommodate trends in the oxidation of the constituent elements. The oligomerization of tin telluride clusters and the cross-linking through platinum ions combine to yield a material that shows a continuous and gradual change in the tin oxidation state. This, in turn, leads to gradual changes in the band gap (0.57−0.75 eV), the conductivity (0.0086−0.0057 $\Omega^{-1}\cdot$cm^{-1}), and the absolute valence band energies (−5.8 to −5.1 eV) as the chemical composition is altered. While trends in band gap have been observed previously by tuning the elements used to produce these composites, the ability to modify materials by changing the oxidation state of the metal cross-linking salt offers a new way to tune the electronic structure.[20−28]

Moreover, because a series of isostructural composites can be produced, these materials give us a unique opportunity to examine some of the details of the electronic structures of these materials. For example, the consistency in the value of the pore capacitance across samples determined by impedance spectroscopy (Figure 8) suggests that such capacitance effects may be intrinsic to nanoperiodic composite semiconductors. The trends in band gap and in conductivity can also be used in combination

(42) Clark, A. H.; Burke, T. J. *Phys. Rev. Lett.* **1972**, *28*, 678.

with simple models of thermally activated carriers to learn more about carrier mobility in these unique nanoscale semiconductors. Finally, optical band gap information can be combined with valence band energies to paint a full picture of the accessible filled and empty electronic energy levels in these materials.

1. Impedance Analysis. In addition to the chemical control over electronic properties, the physical properties of these semiconductors are influenced by the nanoscale architecture. The organic structure directing agent in these composites provides a dielectric interface in the materials that leads to a capacitance which is a function of the periodicity. The pore capacitance model presented here is based on the concept that if there is a polarizable medium, in this case, the organic structure directing agent, embedded in a semiconductor, there will be a build up of charge in the semiconductor at this semiconductor/insulator interface. The capacitance can be calculated using the equation below using the assumption that the organic templating agent can be modeled as a dielectric cylindrical core (see Supporting Information for a full derivation)

$$C_{\text{pore}} = \left(\frac{z \times \epsilon_0(\epsilon_{\text{pore}} - 1)}{2}\right)\left(\frac{\epsilon_{\text{pore}}}{\epsilon_{\text{semicon}}}\right) \quad (1)$$

where the length of the cylinder is z; ϵ_0 is the permittivity of free space, and ϵ_{pore} and $\epsilon_{\text{semicon}}$ are the dielectric constant of the organic core and inorganic semiconductor framework, respectively. The calculated pore capacitance for eq 1 was derived by dividing the charge built up on the cylindrical dielectric core by the potential drop across the pore; both charge and potential drop were derived classically and are included in the Supporting Information.

To scale-up a single pore capacitance into the capacitance of a three-dimensional grain, an assumption was made that the dielectric of the organic confined within the pores does not interact with current traveling through the Pt−$SnTe_4$ framework parallel to the long axis of the pores. Therefore, the total contribution to the capacitance of a single grain arises from current traveling through the Pt−$SnTe_4$ framework perpendicular to the length of the pores. Consequently, the effective capacitance of a single grain arises from the two-dimensional arrangement of the pores in a hexagonal close-packed structure, which has approximately as many pore capacitors in parallel as there are in series. Because of cancellation of parallel and series capacitors, we find that the effective capacitance of a grain (C_{grain}) is approximately equal to the pore capacitance (C_{pore}) in this two-dimensional hexagonal close-packed structure.

The system's total capacitance was found by taking the calculated capacitance for a grain (C_{grain}) and scaling it up using the dimensions of the impedance measurement cell. Assuming the grain size is 0.001 μm^3, 3×10^8 grains exist in parallel in the measurement cell with a cross-sectional area of 0.03 cm^2. To contribute to the total capacitance, a grain's pores must align perpendicular to the applied electric field. On average, only $^2/_3$ of the total grains contribute additively to the total capacitance.[43] This gives rise to a parallel capacitance from the impedance measurement cell of

$$C_{\text{grain}} \times 3 \times 10^8 \times \frac{2}{3} = 2 \times 10^8 C_{\text{grain}} \quad (2)$$

The number of grains packed linearly along the length (0.15 cm) of the impedance measurement cell is approximately 1.5×10^4, and these grains are in series and contribute inversely to the total capacitance. Therefore, the total capacitance becomes

$$C_{\text{total}} = \frac{2 \times 10^8 C_{\text{grain}}}{1.5 \times 10^4} = \frac{2 \times 10^8}{1.5 \times 10^4} \frac{z \times \epsilon_0(\epsilon_{\text{pore}} - 1)}{2}\left(\frac{\epsilon_{\text{pore}}}{\epsilon_{\text{semicon}}}\right) \quad (3)$$

Using the above equation, the total pore capacitance is found to be $\sim 1 \times 10^{-12}$ F using dielectric constants of 40 and 9 for the organic structure directing agent and semiconductor, respectively. The value of 40 for the organic-phase dielectric comes from examining all of the organic components of the composite. The dielectric constant of the surfactant, cetyltriethylammonium ($CTEA^+$, 10), is approximated by averaging the dielectric constants of ammonium iodide (9.8), ammonium nitrate (10.7), and ammonium sulfate (10.0).[34] Elemental analysis, however, indicates that the organic portions of the Pt(II) cross-linked composite are composed of 40% formamide and 60% $CTEA^+$. The dielectric constant of formamide is 84.[34] The dielectric constant of the platinum tin telluride semiconductor was estimated to be 9 by averaging the dielectric constants of a number of chalcogenide-containing semiconductors, including ZnS (8.9), ZnSe (9.2), ZnTe (10.4), and CdTe (7.2).[34] The experimental total pore capacitance (1.8×10^{-12} F) agrees qualitatively with the calculated capacitance (1×10^{-12} F), supporting the validity of the physical model used to determine the equivalent circuit. The results thus indicate that a complex nanoscale architecture can have a dramatic effect on the electrical properties of a composite material and can effect both resistive and capacitive aspects of materials conductivity.

2. Carrier Mobility. The trends in conductivity across the inorganic/surfactant self-assembled Pt−$SnTe_4$ composite series also imply trends in carrier mobility within these semiconductors. While the conductivity decreases as the band gap increases, the decrease in conductivity is not an exponential function of the band gap, as would be expected for a semiconductor where thermal excitation governs conductivity. This implies that an increase in both the mobility and band gap in these nanoscale composites counteracts this expected exponential decrease in conductivity. We note that to draw quantitative conclusions about changes in mobility based on the conductivity, it is necessary to assume that only the band structure changes as the ratio of Pt(IV):Pt(II) is altered, and this change in platinum oxidation state does not result in doping of the nanoscale semiconductor. A simple doping model would require similar structures with differing amounts of organic counterions to account for the doping, however, and elemental analysis shows a fairly consistent organic mass fraction across all samples. This supports a model that the electronic structure of the framework changes due to a combination of tin telluride cluster oligomerization, varying incorporation of platinum, and changes in oxidation state of the tin atoms, all of which should directly affect the band structure of the materials.

The mobility (μ) of carriers was calculated using the band gap and conductivity of the semiconducting platinum tin

(43) Approximate grain size as determined from transmission electron microscopy.

telluride inorganic/organic composites. To determine a trend in the mobility of carriers in these semiconducting composite materials, an estimate of the number of condition band electrons and valence band holes is needed. For an intrinsic semiconductor, the number of conduction band electrons and valence band holes are the same and are given a common value N, which is a function of the band gap and temperature, and the effective mass of the carriers is as seen in eq 4 below

$$N = 2\left(\frac{2\pi \times k_b T}{h^2}\right)^{3/2} (m_e m_h)^{3/4} e^{(-Eg/2k_b T)} \quad (4)$$

where k_b is Boltzmann constant; T is temperature; m_e and m_h are the effective electron mass and hole mass, respectively, and E_g is the band gap.[44] The effective mass of the electrons and holes is needed to calculate N. Unfortunately, these numbers could not be determined experimentally, so their values were estimated.

The electronic effective mass was estimated using the empirical relationship

$$\frac{m_e}{m} = E_g \times \text{constant} \quad (5)$$

where m is the electron rest mass.[44] The constant in eq 5 is found to be 0.07 ± 0.015 based on averaging over the following intrinsic direct band gap semiconductors: GaSb, GaAs, InSb, InAs, InP, CdS, CdSe, and ZnO.[45] This constant along with the experimental band gap (E_g) is used to approximate the effective mass of electrons in the series of Pt−$SnTe_4$ composites. Hole masses show less dependence on band gap, and in fact, the average effective mass of the holes in these intrinsic direct band gap semiconductors is found to be 0.5 ± 0.2. This value is thus used to approximate the effective mass of holes in these composites.[45] While these are very rough estimates, they do not need to be perfect to allow us to draw trends about mobility. We estimate that if N can be determined within an order of magnitude, then robust trends in mobility can be obtained. The total mobility, which is the sum of electron and hole mobility for an intrinsic semiconductor, is calculated using the following relation

$$\sigma = 2Ne(\mu_e + \mu_h) \quad (6)$$

where σ is the conductivity; μ_e is the electron mobility, and μ_h is the hole mobility.[44]

The calculated total mobility for the semiconducting platinum tin telluride framework increases in value from 3×10^3, 9×10^3, and 2×10^4 to 5×10^4 $cm^2 \cdot V^{-1} \cdot s^{-1}$ as the Pt(IV) content is increased for samples with Pt(IV):Pt(II) molar ratios of 0:4, 1:3, 2:2, and 4:0, respectively. Larger mobilities were observed as the amount of Pt(IV) incorporated into the structure is increased. This may be due to an increase in tellurium bridging in the material. The $SnTe_4^{4-}$ anion is oligomerized to larger SnTe clusters as the Pt(IV) content increases, leading to more chalcogenide bridging. The result indicates that minimizing metal ion content may lead to the highest mobility structures. This idea is supported by recent results that show that chalcogenide clusters such as these can lead to very high mobility materials when thermally condensed in the absence of any metal.[46] Recent results indicate that such metal-free cross-linking may also be possible in nanostructured surfactant-templated materials.[47]

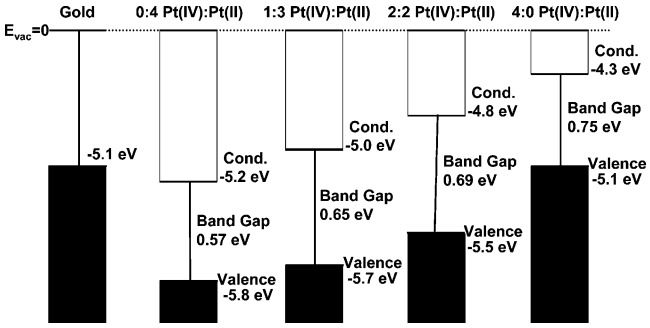

Figure 10. A summary of the energy levels obtained from near-IR/UV−visible diffuse reflectance measurements and ultraviolet photoelectron spectroscopy for the mesostructured platinum tin telluride inorganic/surfactant composites as a function of the Pt oxidation state used in the synthesis. The absolute energy levels of the upper edge of the valence band (black box) and the lower edge of the conduction band (white box) are shown in the figure along with the band gap of these composites. As the amount of Pt(IV) incorporated into the mesostructured composite is increased, the conduction band edge can be tuned by almost 0.9 eV while changing the band gap by only ~0.2 eV.

3. Band Structure. The conduction band edge on an absolute energy scale can be determined from the absolute valence band edge and the band gap of a material. The absolute energy of the valence band edge for these composites is determined through ultraviolet photoelectron spectroscopy (Figure 9). Visible/near-IR reflectance spectroscopy (Figure 4) is used to determine the optical band gap. A summary of the accessible valence and conduction band energy levels obtained from the experimental data for the series of platinum tin telluride/surfactant composites is shown in Figure 10. As the platinum(IV) content in the synthesis mixture is increased, the absolute energy of both the valence and the conduction band edges moves up toward the vacuum level. The source of this shift in absolute energy is related to the varying stoichiometry of the different composites and the atomic makeup of the valence and conduction bands.

We have established that the elemental composition can be tuned by varying the amount of Pt(IV) used in the synthesis of each mesostructured composite (Figure 3 and Table 1). Generally speaking, materials made with more Pt(II) contain a higher elemental fraction of Te and Pt, while those made with Pt(IV) contain less Te and Pt and more Sn. Examination of band structure calculations for chalcogenide semiconductors suggests how these elemental trends can result in both the observed conduction and valence band shifts (Figure 10).[48,49] Density of states (DOS) calculations show that the valence band is dominated by chalcogenide nonbonded p-orbitals.[48,49] Experimental studies on Pb−Se−In chalcogenide glasses further show

(44) Kittel, C. *Introduction to Solid State Physics*, 7th ed.; Wiley: New York, 1996.
(45) Sze, S. M. NetLibrary Inc. *Physics of Semiconductor Devices*, 2nd ed.; Wiley: New York, 1981.
(46) Mitzi, D. B.; Kosbar, L. L.; Murray, C. E.; Copel, M.; Afzali, A. *Nature* **2004**, *428*, 299.
(47) Riley, A. E.; Tolbert, S. H. Synthesis and Characterization of Tin Telluride Inorganic/Organic Composite Materials with Nanoscale Periodicity through Solution Phase Self-Assembly: A New Class of Composite Materials Based on Zintl Cluster Self-Oligomerization. *Res. Chem. Intermed.* In press.
(48) Polatoglou, H. M.; Theodorou, G.; Economou, N. A. *Phys. Rev. B* **1986**, *33*, 1265.
(49) Lazaro, S. D.; Longo, E.; Sambrano, J. R.; Beltran, A. *Surf. Sci.* **2004**, *552*, 149.

that this p-band shifts to higher energy as more group IV elements are added to the material.[50] The shift is explained by destabilization of the lone pair p-orbitals by electropositive group IV elements.[50] In agreement with this idea, an increase in valence band energy is observed with increasing Sn content in hexagonal nanostructured composites (Figure 10).

DOS calculations further indicate that the conduction band is formed predominantly from group IV p-orbitals.[48] Experimentally, the addition of metals to a chalcogenide glass has been shown to add states at the edge of the conduction band, effectively lowering the conduction band energy.[51] For example, in Se−Te−As−Ge semiconducting glasses doped with nickel metal, the conduction band edge shifted to lower energy as the concentration of nickel increases. In our hexagonal nanoscale composites, we see the same trend of decreasing conduction band edge energy with increasing Pt content (Figure 10). The ability to control the relative composition of Pt, Sn, and Te thus allows us to tune the absolute valence and conduction band energies.

Moreover, because of charge neutrality constraints, we find that shifts in valence on conduction band energies are correlated. Higher Pt content is accompanied by a higher Te and lower Sn content, thus decreasing the energy of both the valence and conduction band. In the end, the valence band energy can be shifted by ∼0.7 eV, while the conduction band energy shifts by ∼0.9 eV. Both of these values are much larger than the ∼0.2 eV shift in the band gap that occurs when changing the amount of Pt(IV) used in the synthesis of these mesostructured composite. For a broad range of applications where current is injected into a material or generated by a material (solar cells, LEDs, FETs), semiconductor energy levels need to be tuned to match relevant electrodes or other chromophores.[52−55] Moreover, it is desirable to be able to tune these energy levels while only minimally changing the band gap, as the gap is often chosen to emit or absorb a specific color of light. These results show that tuning of absolute energy levels is possible using simple chemical manipulation in these flexible nanoscale composite materials.

Conclusions

The novel synthetic method of varying the oxidation state of the metallic cross-linking components incorporated into chalcogenide composites allows perturbations to the electronic structure while maintaining the basic molecular building blocks and the nanoscale order. It has been shown that the band gap, conductivity, and absolute energy levels of the Pt/Sn/Te/surfactant composites can be fine tuned by varying the platinum oxidation states using combinations of Pt(II) and Pt(IV) salts in the synthesis. The inorganic/organic composites form small band gap semiconductors that have reasonable conductivity, making them potentially useful in devices which take advantage of intrinsic semiconductor conductivity. Additionally, simple solution-phase processing, the ability to tune the band gap, and the ability to tune the absolute energy levels of these materials make them even more attractive candidates for devices.

To truly take advantage of the electronic tunability in these materials, however, one would like to remove the surfactant to produce periodic nanoporous semiconductors. For surfactant-templated silica-based materials, where surfactant can be removed to produce porous inorganics,[1,56] one advantage of the nanoscale honeycomb architecture is that disparate materials can be intimately mixed by putting guests in pores.[57−62] For device applications, the specific goal is to incorporate optically and electronically active guests into the pores.[57−66] Guest incorporation in these templated Pt−$SnTe_4$ semiconducting materials could be used to form such interesting species as nanoscale semiconductor−semiconductor heterojunctions. Unfortunately, to date, surfactant removal from these materials to produce mesoporous semiconductor has not been possible. Therefore, to exploit the tunable electronic properties in these nanoscale materials, functionality must be incorporated into the organic domains during synthesis in order to make useful devices.

There are a variety of methods that have been employed to accomplish this goal. A range of optically active guests can simply be mixed with the surfactant template and incorporated into the hydrophobic region of the organic domains.[67,68] While such a guest could lead to light emission, they cannot generally form a second conducting phase. To produce a semiconducting organic domain, amphiphilic semiconducting polymers have been employed as templates, which should enable conductivity throughout the pore system of the structure.[69] Alternatively, polymerizable surfactants or monomers can be cross-linked to form a conductive polymer within the framework after self-organization.[70,71] To date, these direct incorporation methods have been applied only to insulating oxide systems,[69−71] but Pt−$SnTe_4$ materials offer a unique advantage as a narrow band gap nanostructured semiconductor. By incorporating electronic functionality into the organic structure directing agent, the electronic tunability of these Pt−$SnTe_4$ self-assembled structures

(50) Mehra, R. M.; Sandeep, K.; Pundir, A.; Sachdev, V. K.; Mathur, P. C. *J. Appl. Phys.* **1997**, *81*, 7842.
(51) Gomi, T.; Hirose, Y.; Kurosu, T.; Shiraishi, T.; Iida, M.; Gekka, Y.; Kunioka, A. *J. Non-Cryst. Solids* **1980**, *41*, 37.
(52) Grätzel, M. *Nature* **2001**, *414*, 338.
(53) Huynh, W. U.; Dittmer, J. J.; Alivisatos, A. P. *Science* **2002**, *295*, 2425.
(54) Meijer, E. J.; de Leeuw, D. M.; Setayesh, S.; van Veenendaal, E.; Huisman, B. H.; Blom, P. W. M.; Hummelen, J. C.; Scherf, U.; Kadam, J.; Klapwijk, T. M. *Nat. Mater.* **2003**, *2*, 834.
(55) Tessler, N.; Medvedev, V.; Kazes, M.; Kan, S. H.; Banin, U. *Science* **2002**, *295*, 1506.
(56) Zhao, D.; Feng, J.; Huo, Q.; Melosh, N.; Fredrickson, G. H.; Chmelka, B. F.; Stucky, G. D. *Science* **1998**, *279*, 548.
(57) Nguyen, T. Q.; Wu, J. J.; Doan, V.; Schwartz, B. J.; Tolbert, S. H. *Science* **2000**, *288*, 652−656.
(58) Molenkamp, W. C.; Watanabe, M.; Miyata, H.; Tolbert, S. H. *J. Am. Chem. Soc.* **2004**, *126*, 4476.
(59) Gross, A. F.; Diehl, M. R.; Beverly, K. C.; Richman, E. K.; Tolbert, S. H. *J. Phys. Chem. B* **2003**, *107*, 5475.
(60) Hirai, T.; Okubo, H.; Komasawa, I. *J. Phys. Chem. B* **1999**, *103*, 4228.
(61) Zhou, W. Z.; Thomas, J. M.; Shephard, D. S.; Johnson, B. F. G.; Ozkaya, D.; Maschmeyer, T.; Bell, R. G.; Ge, Q. F. *Science* **1998**, *280*, 705.
(62) Nagl, I.; Widenmeyer, M.; Grasser, S.; Köhler, K.; Anwander, R. *J. Am. Chem. Soc.* **2000**, *122*, 1544.
(63) Crowley, T. A.; Ziegler, K. J.; Lyons, D. M.; Erts, D.; Olin, H.; Morris, M. A.; Holmes, J. D. *Chem. Mater.* **2003**, *15*, 3518.
(64) Gu, J.; Shi, J.; Xiong, L.; Chen, H.; Li, L.; Ruan, M. *Solid State Sci.* **2004**, *6*, 747−752.
(65) Fukuoka, A.; Miyata, H.; Kuroda, K. *Chem. Commun.* **2003**, 284.
(66) Wang, D. W.; Zhou, W. L.; McCaughy, B. F.; Hampsey, J. E.; Ji, X. L.; Jiang, Y. B.; Xu, H. F.; Tang, J. K.; Schmehl, R. H.; O'Connor, C.; Brinker, C. J.; Lu, Y. F. *Adv. Mater.* **2003**, *15*, 130.
(67) Wu, J. J.; Abu-Omar, M. M.; Tolbert, S. H. *Nano Lett.* **2001**, *1*, 27.
(68) Belhadj Miled, O.; Grosso, D.; Sanchez, C.; Livage, J. *J. Phys. Chem. Solids* **2004**, *65*, 1751.
(69) Clark, A. P.; Shen, K.; Rubin, Y.; Tolbert, S. H. Amphiphilic Poly(phenylene ethynylene) as the Structure-Directing Agent for Nanostructured Silica Composite Materials. *Nano Lett*. Submitted.
(70) Lu, Y.; Yang, Y.; Sellinger, A.; Lu, M.; Huang, J.; Fan, H.; Haddad, R.; Lopez, G.; Burns, A. R.; Sasaki, D. Y.; Shelnutt, J.; Brinker, C. J. *Nature* **2001**, *410*, 913.
(71) McCaughey, B.; Costello, C.; Wang, D. H.; Hampsey, J. E.; Yang, Z. Z.; Li, C. J.; Brinker, C. J.; Lu, Y. F. *Adv. Mater.* **2003**, *15*, 1266.

may find uses in applications, such as photovoltaic devices or field effect transistors.[72]

Acknowledgment. We would like to thank Il-Sup Jin for help with impedance spectroscopy. XANES data were collected at the Stanford Synchrotron Radiation Laboratory (SSRL), and UPS data were collected at the Advanced Light Sources (ALS), both of which are operated by the Department of Energy, Office of Basic Energy Science. This work was supported by the National Science Foundation (Grant CHE-9985259) and by the Office of Naval Research (Grant N00014-04-1-0410). S.H.T. is an Alfred P. Sloan Foundation Research Fellow.

Supporting Information Available: Detailed derivation of the capacitance induced by the organic structure directing agent, which is a dielectric cylindrical core imbedded in a semiconductor (eq 1). This material is available free of charge via the Internet at http://pubs.acs.org.

JA045446K

(72) Coakley, K. M.; McGehee, M. D. *Appl. Phys. Lett.* **2003**, *83*, 3380.